**HIGHLIGHT**

# Phonon engineering through crystal chemistry†

Eric S. Toberer,* Alex Zevalkink and G. Jeffrey Snyder*

Mitigation of the global energy crisis requires tailoring the thermal conductivity of materials. Low thermal conductivity is critical in a broad range of energy conversion technologies, including thermoelectrics and thermal barrier coatings. Here, we review the chemical trends and explore the origins of low thermal conductivity in crystalline materials. A unifying feature in the latest materials is the incorporation of structural complexity to decrease the phonon velocity and increase scattering. With this understanding, strategies for combining these mechanisms can be formulated for designing new materials with exceptionally low thermal conductivity.

## Introduction

Controlling heat flow is critical to applications ranging from jet turbines to microelectronics to thermoelectrics. In energy applications, thermal engineering frequently determines system efficiency, lifetime, and cost. For example, thermal barrier coatings enable higher turbine operating temperature, thereby increasing the Carnot efficiency.[1–3] In thermoelectrics, dramatic improvements in efficiency have been driven by reductions in thermal conductivity.[4–8] The discovery of complex, bulk thermoelectric materials with low thermal conductivity (*e.g.*, $Yb_{14}MnSb_{11}$, $Ba_8Ga_{16}Ge_{30}$, $X_yCo_4Sb_{12}$) has led to a renewed investigation of the fundamental mechanisms of thermal conductivity.[14–17] Similar low thermal conductivity has been found in thermal barrier coating materials ($La_2Mo_2O_9$, $W_3Nb_{14}O_{44}$).[18]

Understanding the origins of this behavior is important for the development of advanced materials. The complexity of these materials, however, makes *ab initio* calculations of lattice dynamics prohibitively difficult.[19–24] Here

*Materials Science, California Institute of Technology, 1200 E, California Blvd. PasadenaCA, 91125, USA. E-mail: etoberer@mines.edu; jsnyder@caltech.edu*
† Electronic supplementary information (ESI) available: Supplementary Table 1. See DOI: 10.1039/c1jm11754h
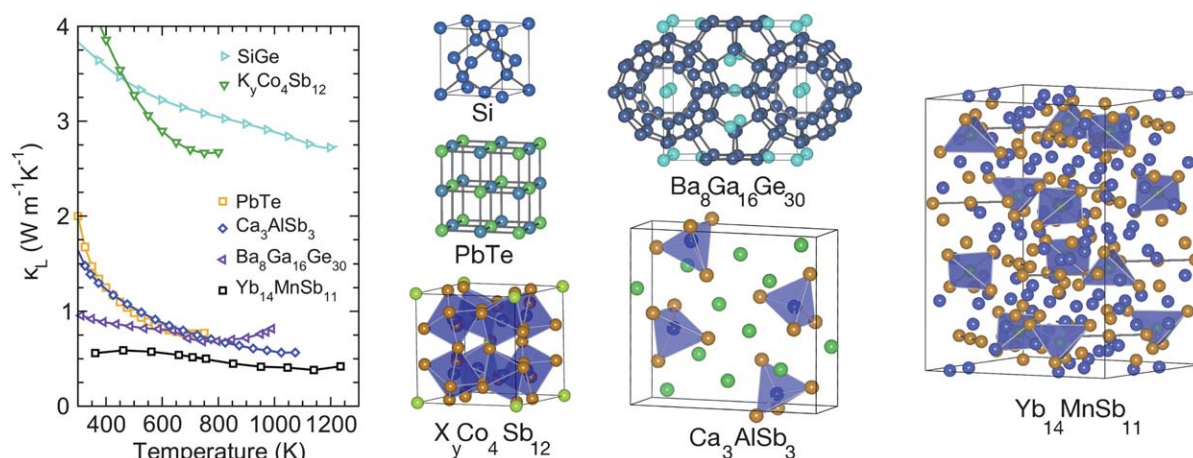
we use simple models for heat transport to approximate the complex interplay of phonon scattering and group velocity. Despite these approximations, these models highlight the critical *material parameters* that ultimately determine thermal conductivity.

Thermal conductivity in a material arises from both electronic ($\kappa_e$) and lattice ($\kappa_L$) contributions.[25–28] The electronic component is well described by the Wiedemann–Franz law, scaling linearly with the electrical conductivity and temperature. The lattice contribution arises from lattice vibrations (phonons) and is the subject of this review.

To lay the groundwork for a more in-depth examination of factors affecting lattice thermal conductivity, we consider eqn (1), which describes $\kappa_L$ as the product of heat capacity ($C_v$), phonon velocity ($v$), and phonon mean free path ($l$). This equation provides a rough guide to $\kappa_L$, despite neglecting the frequency dependence of each parameter. The phonon relaxation time, $\sigma$, is related to $l$ through the phonon velocity. The phonon velocity is often simply approximated by the low frequency speed of sound ($v_s \propto \sqrt{B/\delta}$), where $B$ is the appropriate elastic modulus and $\delta$ is the density of the material.

$$\kappa_L = \frac{1}{3}C_v v l = \frac{1}{3}C_v v^2 \tau \quad (v = l/\tau) \quad (1)$$

Traditionally, achieving low lattice thermal conductivity has relied on (a) low $v_s$, found in dense materials with soft bonds, or (b) reduction of $\sigma$ by the intentional introduction of point defects and nanostructures to scatter phonons.[1,9,10,29–32] Fig. 1 shows the success of these approaches in thermoelectric materials.

While eqn (1) qualitatively describes $\kappa_L$, the universal relaxation time and constant velocity used in this model leads to significant inconsistencies and departure from experimental results. Crucial to the development of materials with controlled phonon transport is a frequency-dependent description of $\kappa_L$, as all of the terms in eqn (1) vary significantly across the phonon spectrum. Use of a simplified version of the Callaway model gives eqn (2),[33,34] which neglects the small correction term for non-resistive (normal) phonon–phonon interactions.[19,20,26,35]

$$\kappa_L = \frac{1}{3}\int_0^{\omega_{max}} C_s(\omega)v_g(\omega)^2\tau(\omega)d\omega \quad (2)$$

The need for frequency-dependent analysis is revealed by considering bulk silicon. Eqn (1) yields $l = 45$ nm at 300 K, using experimental $\kappa_L$, heat capacity, and speed of sound. In contrast, eqn (2) indicates that 80% of the lattice thermal conductivity arises from phonons with mean free paths between 0.1–10 μm.[36] This latter result is consistent with

This journal is © The Royal Society of Chemistry 2011

*J. Mater. Chem.*, 2011, **21**, 15843–15852 | 15843

**Fig. 1** Thermoelectric materials can achieve low lattice thermal conductivity through point scattering sources ($Si_{1-x}Ge_x$, $X_yCo_4Sb_{12}$), heavy atoms and anharmonic bonding (PbTe) and complex crystal structures, in which most of the phonon dispersion consists of low velocity optical modes ($Yb_{14}MnSb_{11}$, $Ca_3AlSb_3$, $Ba_8Ga_{16}Ge_{30}$).[9–14]

experimental results which show significant reduction in $\kappa_L$ when phonon scattering sources are induced at micron length scales.[37]

Here we review the frequency dependence of scattering and highlight the importance of the phonon dispersion in determining $\kappa_L$. We begin with a discussion of the *prediction* of lattice thermal conductivity in simple materials where the phonon group velocity can be approximated as constant (Debye model). We then use this understanding to tackle more complex materials where the group velocity is highly frequency-dependent. These examples guide the design and discovery of low thermal conductivity materials.

## Thermal conductivity within the Debye model

The Debye model is a reasonable starting point for discussing thermal transport in simple crystalline materials, as it allows us to approximate the phonon group velocity ($\nu_g = d\omega/dk$) and phase velocity ($\nu_p = \omega/k$) as the speed of sound, $\nu_s$ (Fig. 2).[38,39] Here, $\nu_s$ is the appropriate average of the longitudinal and transverse velocities at the low frequency limit. The Debye model has a maximum phonon frequency given by $\omega_{max} = \omega_D = \left(\frac{6\pi^2}{V}\right)^{1/3} \nu_s$, where $V$ is the atomic volume. The corresponding Debye temperature is given by $k_B\theta_D = \hbar\omega_D$.

The Debye specific heat capacity is given by eqn (3). We are interested in the *spectral* heat capacity ($C_s(\omega)$), related to the phonon density of states, shown in Fig. 3(a) at various temperatures. At high temperature, the frequency dependence of $C_s(\omega)$ approaches $\omega^2$ and can be approximated by eqn (4). Integrating eqn (4) to $\omega_D$ yields the Dulong Petit approximation ($3k_B$ per atom) for the heat capacity.

$$C_v = \frac{3\hbar^2}{2\pi^2 k_B T^2} \int_0^{\omega_{max}} \frac{\omega^4 e^{\hbar\omega/k_B T}}{\nu_g \nu_p^2 (e^{\hbar\omega/k_B T} - 1)^2} d\omega \quad (3)$$

$$C_{s,HT}(\omega) = \frac{3k_B\omega^2}{2\pi^2 \nu_g \nu_p^2} \quad (4)$$

We now consider the frequency dependence of the phonon relaxation time, $\sigma(\omega)$.[40] Thermal conductivity is typically limited by a combination of phonon–phonon scattering, point defect scattering and, in nanostructured materials, boundary scattering, which sum according to eqn (5).

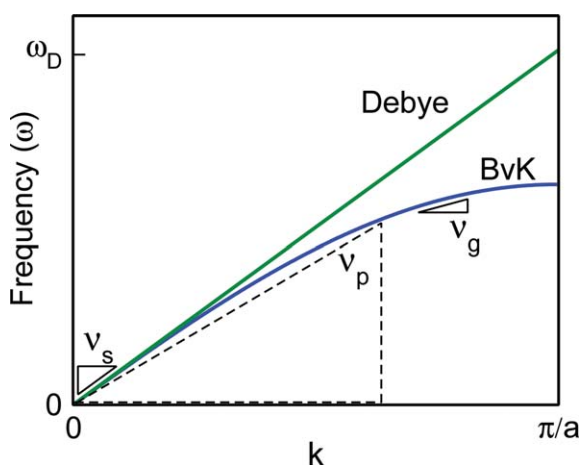$$\tau^{-1} = \sum_i \tau_i^{-1} \quad (5)$$



**Fig. 2** In a Debye model, the speed of sound ($\nu_s$), phase velocity ($\nu_p$), and group velocity ($\nu_g$) are equivalent. In contrast, a simple Born–von Karman model shows significant curvature of the phonon dispersion.

**Variables:**

| | |
|---|---|
| $\kappa_L$ | lattice thermal conductivity |
| $\kappa_s(\omega)$ | spectral lattice thermal conductivity |
| $C_v$ | heat capacity |
| $C_{s,HT}(\omega)$ | high temperature spectral heat capacity |
| $\nu_g(\omega)$ | phonon group velocity, $d\omega/dk$ |
| $\nu_p(\omega)$ | phonon phase velocity, $\omega/k$ |
| $\nu_s$ | averaged speed of sound |
| $\sigma$ | phonon relaxation time |
| $\bar{M}$ | average mass |

| | |
|---|---|
| $V$ | volume per atom |
| $\gamma$ | Grüneisen parameter |
| $d$ | grain or microstructure size |
| $N$ | atoms per primitive cell |
| $\omega$ | phonon frequency |
| $k$ | wave vector |
| $a$ | lattice parameter |

At temperatures above $\theta_D$, Umklapp phonon-phonon scattering is often the dominant scattering effect. Umklapp scattering depends strongly on the anharmonicity of the bonding, described by the Grüneisen parameter ($\gamma$),[41,42] as well as the average mass ($\bar{M}$), and temperature ($T$), as seen in eqn (6). Although many expressions exist for $\sigma_U$, we emphasize the universality of $\tau_U \propto \dfrac{\bar{M}v^3}{V^{1/3}\omega^2\gamma^2 T}$ and similarity of the pre-factor.[35,43–46] It is instructive to consider the rock salt compounds PbTe and PbSe in the context of eqn (6). While heavier, softer PbTe has a lower group velocity than PbSe, the larger Grüneisen parameter of PbSe leads to similarly low $\kappa_L$.[47]

$$\tau_U(\omega) = \frac{(6\pi^2)^{1/3}}{2} \frac{\bar{M}v_g v_p^2}{k_B V^{1/3}\gamma^2\omega^2 T} \quad (6)$$

Boundary scattering in polycrystalline materials with grain size $d$ can be estimated from eqn (7).[48,49] This scattering mechanism is particularly effective in nanostructured materials such as nanowires, thin films, and nanocomposites.[29–31,50]

$$\tau_B = \frac{d}{v_g} \quad (7)$$

Scattering by point defects arises from both mass and strain contrast within the lattice. Point defect scattering has been successfully employed in both thermoelectric materials ($Si_{1-x}Ge_x$), and in thermal barrier coatings, such as yttria stabilized zirconia (YSZ).[1,9] In the simple case of alloying on a single crystallographic site, $\sigma_{PD}$ is given by eqn (8). Here, $f_i$ is the fraction of atoms with mass $m_i$ and radius $r_i$ that reside on a site with average mass and radius $\bar{m}$ and $\bar{r}$, respectively.[39,51]

$$\tau_{PD}^{-1} = \frac{V\omega^4}{4\pi v_p^2 v_g} \left( \sum_i f_i \left( 1 - \frac{m_i}{\bar{m}} \right)^2 \right.$$

$$\left. + \sum_i f_i \left( 1 - \frac{r_i}{\bar{r}} \right)^2 \right) \quad (8)$$

The scattering mechanisms discussed above target different populations of phonons, as shown in Fig. 3(b). Umklapp and point defect scattering target high frequency phonons, while boundary scattering is often the dominant scattering mechanism at low frequencies. In concert, these scattering mechanisms lead to an effective $\sigma$ shown by the dashed line.

The frequency dependence of the phonon contribution to $\kappa_L$ can be used to determine which phonons are critical to
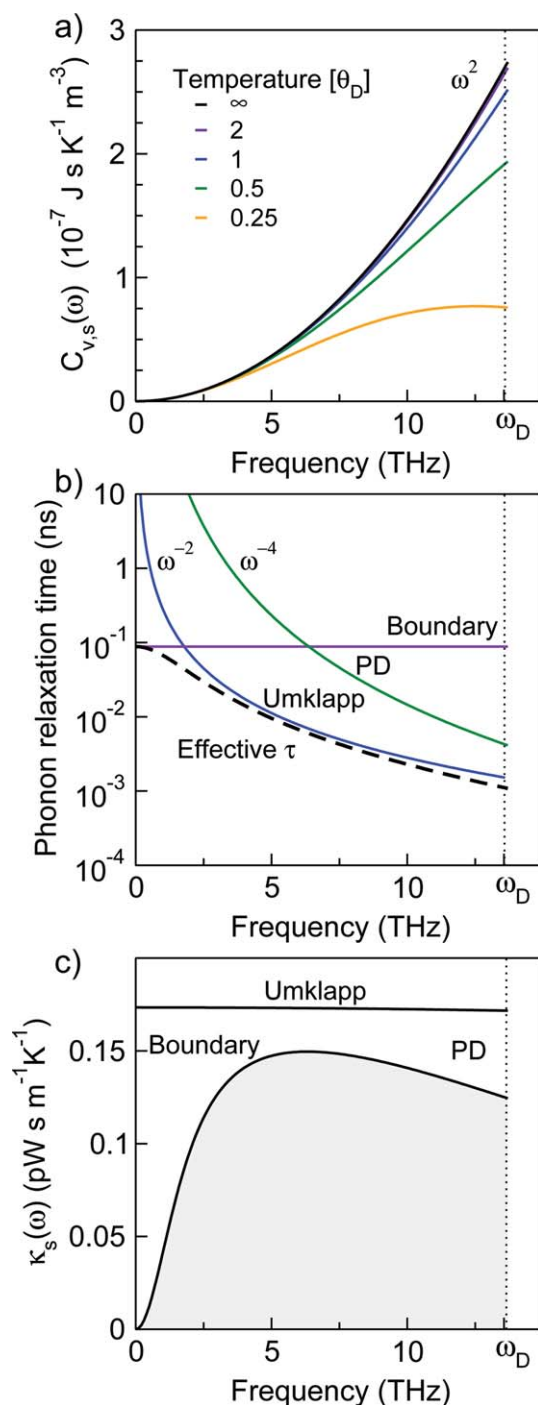


Fig. 3 a) The spectral Debye heat capacity approaches $\omega^2$ dependence at high temperatures. b) Real materials have many scattering mechanisms, which depend heavily on frequency. c) Spectral thermal conductivity (assuming $v_g(\omega) = v_s$ and $T \gg \theta_D$) when Umklapp scattering ($\sigma_U$) dominates transport (top curve) and when $\sigma_U$, $\sigma_B$, and $\sigma_{PD}$ are accounted for (lower curve).

heat transport. The integrand of eqn (2) is commonly referred to as the spectral thermal conductivity, $\kappa_s(\omega) = C_s(\omega) v_g(\omega)^2 \sigma(\omega)$. When thermal conduction is limited by Umklapp scattering, the $\omega^2$ dependence of $C_{s,HT}(\omega)$ is offset by the frequency dependence of Umklapp scattering ($\sigma \propto \omega^{-2}$), resulting in the frequency-independent $\kappa_s(\omega)$ curve shown in Fig. 3(c). Integrating over the phonon spectrum yields the classic expression for $\sigma_U$-limited $\kappa_L$ given in eqn (9).[35,45]

$$\kappa_U = \frac{(6\pi^2)^{2/3}}{4\pi^2} \frac{\bar{M} v_s^3}{TV^{2/3}\gamma^2} \qquad (9)$$

This simple expression is commonly invoked to explain high temperature transport, and yields reasonable estimates for $\kappa_L$ in materials with low mass contrast and simple crystal structures. In most materials, boundary and point defect scattering are also significant, resulting in a highly frequency dependent $\kappa_s(\omega)$. The impact of boundary and point defect scattering on $\kappa_L$ can be readily visualized as the difference in area between the top and bottom curves of Fig. 3(c).

## Thermal conductivity in complex systems

The following sections consider real material systems with phonon dispersions that are progressively more complex than a simple Debye model. Complex phonon dispersions influence $\kappa_L$ by (a) changing the states available for Umklapp scattering and (b) leading to highly frequency-dependent phonon velocities, as $v_g(\omega) = d\omega/dk$.[19,28,52]

Use of a simple Born–von Karman (BvK) model allows us to visualize how chemical structure determines the phonon dispersion. The 1-dimensional BvK model describes the lattice as a chain of atoms connected by springs with harmonic restoring forces.[38,39] Fig. 2 compares the Debye and BvK dispersions for the simple case of a monatomic chain.[53]

**High mass contrast.** The trend between high mass contrast and low lattice thermal conductivity has been clearly demonstrated by Slack.[28] Fig. 4 reveals that the experimental $\kappa_L$ of rock salt

compounds is dramatically overestimated by the Debye model ($\kappa_U$) when mass contrast is high (e.g. BaO, mass ratio of 8.6).

The relationship between mass contrast and $\kappa_L$ can be understood by examining the BvK phonon dispersions for a diatomic chain with varying mass ratio, $m_1 : m_2$ (Fig. 4(b)). When the mass ratio is low, the Debye model's assumption of a constant phonon velocity appears reasonable. However, this assumption breaks down as the mass ratio increases and the optical branch flattens.[54] When $\sigma$

is limited by Umklapp scattering, the spectral thermal conductivity, $\kappa_s(\omega)$, is proportional to $v_g(\omega)^2$. Fig. 4(c) shows the dramatic reduction in $v_g(\omega)^2$, and thus $\kappa_L$, associated with the flattening of the optical modes with increasing mass contrast. Although not accounted for here, changes to the phonon dispersion may also influence the available states for scattering events, leading to changes in the spectral mean free paths.[55]

High mass contrast likely contributes to the low thermal conductivity found in many of the oxides used for thermal
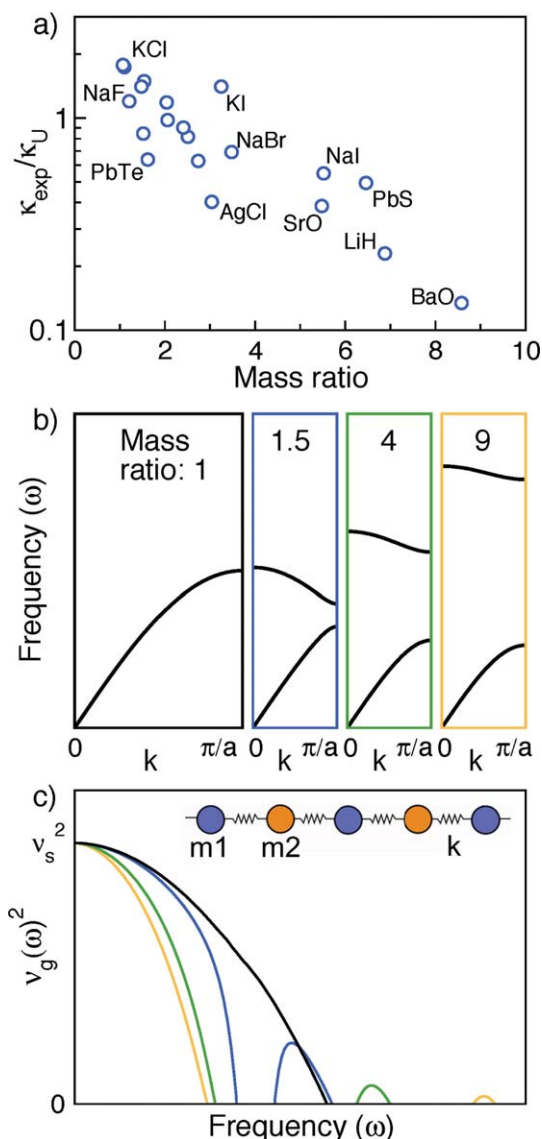


**Fig. 4** a) Calculated $\kappa_U$ significantly overestimates experimental $\kappa_L$ in rock salt compounds with high mass contrast at $T = \theta_D$. Values for $\theta_D$, $\gamma$ and $\kappa_L$ were obtained from Ref. 28. b) This empirical observation can be understood with a BvK model for a 1D diatomic chain. As mass contrast increases (average mass, $v_s$ held constant) the optical mode flattens and the gap increases. c) When Umklapp scattering dominates, $\kappa_s(\omega) \propto v_g(\omega)^2$, and the effect of mass contrast on $\kappa_L$ can be judged from the area beneath the $v_g(\omega)^2$ curves.

**Table 1**

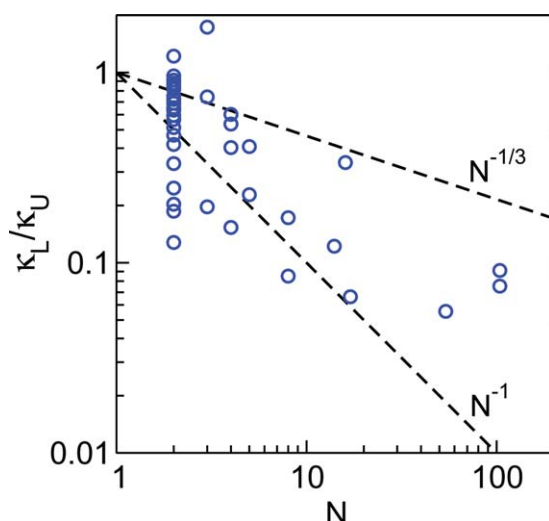| Material | $N$ | $\kappa_L$ (300 K) W/mK | Ref. |
|---|---|---|---|
| $LaPO_4$ | 24 | 2.5 | 18 |
| $W_3Nb_{14}O_{44}$ | 61 | 1.8 | 18 |
| $LaMgAl_{11}O_{19}$ | 64 | 1.2 | 56 |
| $La_2Mo_2O_9$ | 624 | 0.7 | 18 |
| $\alpha\ Al_{14.7}Mn_{3.5}Si_{1.8}$ | 138 | 1.5 | 57 |
| $Ca_5Al_2Sb_6$ | 26 | 1.5 | 58 |
| $Ca_3AlSb_3$ | 28 | 1.6 | 13 |
| $Yb_{11}Sb_{10}$ | 42 | 0.8 | 59 |
| $Yb_{11}InSb_9$ | 42 | 0.8 | 60 |
| $Ba_8Ga_{16}Ge_{30}$ | 54 | 1.1 | 14,16 |
| $Yb_{14}AlSb_{11}$ | 104 | 0.6 | 15 |



**Fig. 5** For materials with many atoms per primitive cell ($N$), eqn (9) fails to predict the experimental $\kappa_L$. See supplemental Table 1.†

barrier coatings (e. g., YSZ has a mass ratio of 5.7). In contrast, most thermo-electric materials have mass contrast less than 2, suggesting a potential avenue for reducing $\kappa_L$.

**Complex primitive cells.** Much like the high mass contrast rock-salt compounds, it has been argued that compounds with a large number of atoms in the primitive unit cell ($N$) have low $\kappa_L$ due to low velocity optical modes.[28,43] Classic examples of high-$N$ compounds with low $\kappa_L$ include $Y_3Al_5O_{12}$ ($N = 80$), $\beta$-Boron ($N = 105$), and $YB_{68}$ ($N = 402$).[28,61] More recently, similar trends has been observed in promising materials for thermoelectrics and thermal barrier coatings (Table 1).[12,18]

To further investigate the trend between low $\kappa_L$ and $N$, we have compiled the properties of materials for which all of the quantities in eqn (9) are known experimentally. Many materials with

applications for thermal barrier coatings have not been included, as their Grüneisen parameters are not reported in the literature. We consider the ratio of measured $\kappa_L$ to that predicted by $\kappa_U$ (eqn (9)). Fig. 5 shows that for simple structures, good agreement between $\kappa_U$ and experimental $\kappa_L$ is observed. However, the $\kappa_L$ of more complex materials is grossly over-estimated by the simple $\kappa_U$ model.

The trend between low $\kappa_L$ and structural complexity can be qualitatively rationalized by a BvK model. Fig. 6(a) shows phonon dispersions for 1D chains with $N$-atom cells. As $N$ increases, the phonon dispersion "folds in" on itself, resulting in $N - 1$ optical modes with low $\nu_g(\omega)$. Thus, in complex materials, the vast majority of heat is trapped in flat, low velocity optical modes, which are not accurately described by a Debye model. Fig. 6(b) emphasizes the reduction of $\nu_g(\omega)^2$ (and thus $\kappa_s(\omega)$ at the limit of

Umklapp scattering), with increasing structural complexity.

For complex materials, a simple approach to modeling $\kappa_L$ is to consider the acoustic ($\kappa_a$) and optical ($\kappa_o$) contributions separately. As seen in Fig. 6(a), the acoustic contribution can be treated within a Debye model. To determine the maximum frequency of the acoustic branch, $\omega_a$, we utilize the equal partition of the heat capacity amongst the phonon modes ($C_{v,acoustic} = C_v/N$), yielding $\omega_a = \omega_D/N^{1/3}$.[43] Values for $\omega_a$ can thus be obtained either from measurements of $\nu_s$ or $\theta_D$. However, when inferring $\omega_a$ from $\omega_D$, the various approaches to obtaining $\theta_D$ (e. g., low or high temperature heat capacity measurements or density of states from neutron experiments) can yield significantly different values.[28,62]

With $\omega_a$ determined, $\kappa_a$ can be determined from eqn (2). For $\sigma$ limited by Umklapp scattering we find $\kappa_a \propto N^{-1/3}$ (eqn (10)). If instead, boundary scattering is assumed to dominate transport, $\kappa_a \propto N^{-1}$ (eqn (11)). For simplicity, we have used the high temperature limit for the heat capacity. In practice, the experimental $N$-dependence in Fig. 5(a) is between these bounds, and is consistent with the $N^{-2/3}$ dependence obtained by Slack.[28]

$$\text{Umklapp}: \kappa_a = \frac{(6\pi^2)^{2/3}}{4\pi^2}\frac{\bar{M}\nu_s^3}{TV^{2/3}\gamma^2}\left(\frac{1}{N^{1/3}}\right) \quad (10)$$

$$\text{Boundary}: \kappa_a = \frac{1}{2}\frac{\nu_s d}{V}\left(\frac{1}{N}\right) \quad (11)$$

At the amorphous limit ($N = \infty$), the acoustic contribution ($\kappa_a$) approaches zero, whereas in practice, glasses still possess finite thermal conductivity. Clearly, we cannot completely ignore the thermal conductivity of the optical modes in which most of the heat in a complex solid is stored. As a lower bound to the optical contribution to thermal conductivity ($\kappa_o$), one can look to Einstein's treatment of heat transport as the diffusion of heat between atomic oscillators. Cahill has extended this theory to larger oscillating units, for which $l_{glass} = \lambda/2$, or equivalently $\sigma_{glass}(\omega) = \pi/\omega$.[63–65] In this model, the speed of sound is used to describe the coupling between oscillators.
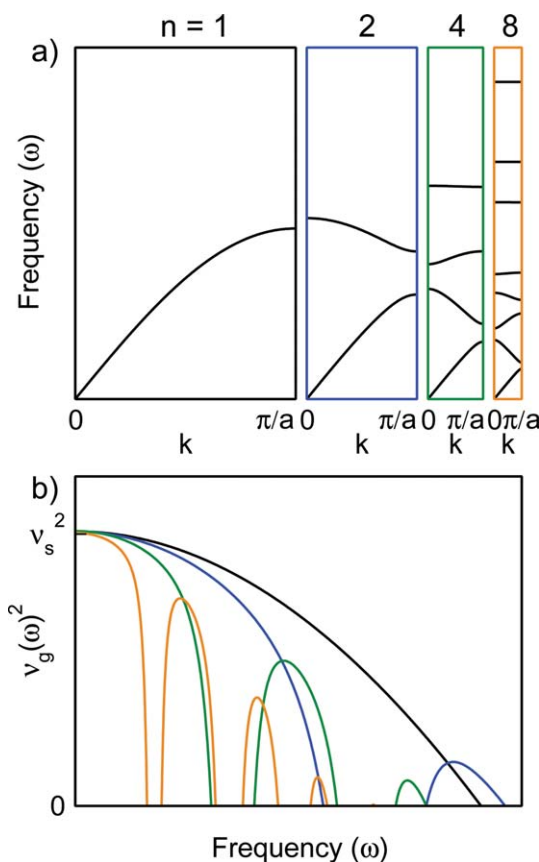
**Fig. 6** a) Phonon dispersions for ball and spring chains with increasing number of atoms per unit cell (constant $\nu_s$). b) A dramatic decrease in $\nu_g(\omega)^2$, and thus $\kappa_s(\omega)$, is found with increasing $N$. For $N = 4$ and 8, the high frequency optical modes are not visible on a linear plot due to the extreme flatness of these modes.

The optical contribution to $\kappa_L$, given by eqn (12), is estimated by evaluating eqn (2) with $\sigma_{glass}$, a minimum optical frequency of $\omega_D/N^{1/3}$, and the high temperature limit to $C_s(\omega)$. We note that our treatment of optical phonons using
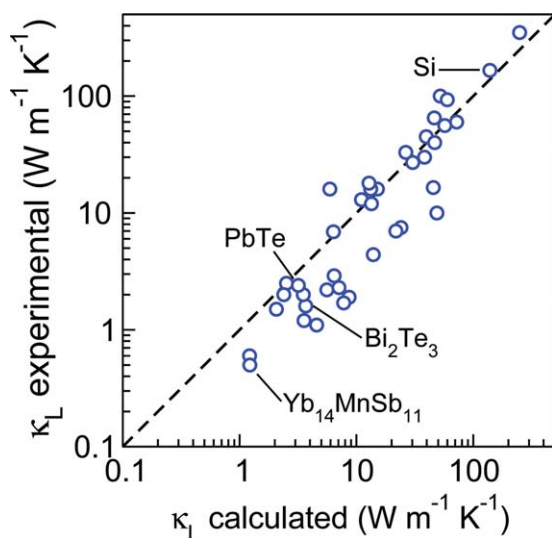
a glass model is somewhat unconventional.[66] Optical branches are generally neglected in the modeling of complex materials.

$$\kappa_o = \frac{3k_B\nu_s}{2V^{2/3}}\left(\frac{\pi}{6}\right)^{1/3}\left(1 - \frac{1}{N^{2/3}}\right) \quad (12)$$

Having developed expressions for both the acoustic and optical phonons, we can re-evaluate the thermal conductivity of the materials presented in Fig. 5. We estimate $\kappa_a$ in a manner analogous to eqn (10) and (11), except that here we assume that both Umklapp and boundary scattering ($d = 1$ μm) limit transport. Summing $\kappa_a$ and $\kappa_o$ (eqn (12)) yields good agreement with the experimental $\kappa_L$ across two orders of magnitude, as illustrated by Fig. 7.

A comparison of $Yb_{14}MnSb_{11}$ and PbTe is particularly revealing. As the bulk properties of these two materials are extremely similar, ($\theta_D$, $\bar{M}$, $C_v$, $\gamma$, see Supplementary Table 1†) $\kappa_U$ suggests that PbTe should have a slightly lower $\kappa_L$ than $Yb_{14}MnSb_{11}$. However, calculations accounting for the difference in $N$ predict that the $\kappa_L$ of $Yb_{14}MnSb_{11}$ ($N = 104$) should be a factor of 3 lower than that of PbTe ($N = 2$) at room temperature. Indeed, the experimental $\kappa_L$ of $Yb_{14}MnSb_{11}$ and PbTe at 300 K are 0.6 and 2 W m$^{-1}$ K$^{-1}$, respectively. The success of this incredibly simple approach to modeling extremely complicated thermal transport processes is inspiring. While computational methods may eventually be able to accurately predict thermal conductivity in complex materials, these methods provide valuable intuition.

In the search for low $\kappa_L$ materials, structural complexity is an elegant approach to achieving glass-like thermal transport across much of the phonon spectrum. Further reduction of thermal conductivity in complex materials can be realized by employing well-established strategies such as: (a) lowering the sound velocity by increasing the density or decreasing the stiffness or (b) including nanostructures to target the remaining acoustic phonons.



**Fig. 7** Success of $\kappa_a + \kappa_o$ in predicting the lattice thermal conductivity of selected materials (see supplementary Table 1†). Here, $\kappa_a$ includes both Umklapp scattering and a boundary scattering term of 1 μm (eqn (5)).

**Rattling modes.** Structural complexity traps heat in glass-like optical modes, but it does not completely eliminate the

15848 | *J. Mater. Chem.*, 2011, **21**, 15843–15852

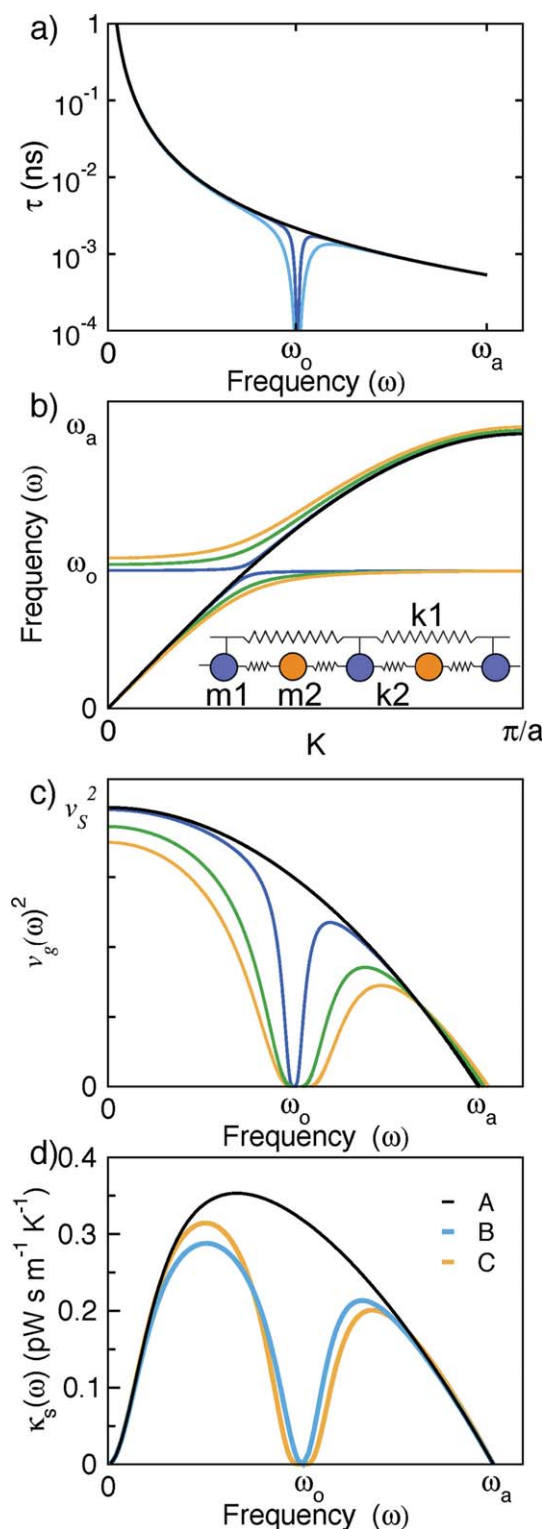This journal is © The Royal Society of Chemistry 2011

**Fig. 8** a) The resonant scattering model targets phonons near $\omega_o$. b) BvK phonon dispersions for a stiff framework ($m_1$, $k_1$) and loosely bound guest atoms ($m_2$, $k_2$). Increased $k_2$ stiffness results in increased coupling (extent of avoided crossing) between the framework and guest modes. c) The avoided crossing reduces $v_g(\omega)^2$ in the vicinity of $\omega_o$. d) $\kappa_s(\omega)$ for an empty BvK framework, using Umklapp and boundary scattering terms (curve A). Including resonant scattering reduces $\kappa_s(\omega)$ near $\omega_o$ (curve B). If instead, the effect of coupling on $v_g(\omega)$ is accounted for, a similar reduction is observed (curve C).

contribution from the high-velocity, acoustic branches. One tactic to reduce the acoustic contribution to thermal conductivity has recently arisen in crystal structures with open-frameworks (*e.g.* clathrates and skutterudites).

Guest insertion into open-framework structures can dramatically affect $C_s(\omega)$, $v_g(\omega)$, and $\sigma(\omega)$. The total heat capacity will increase due to the increased number of atoms per unit volume, potentially increasing $\kappa_L$. The phonon relaxation time, $\sigma$, may be reduced if the guest atoms have highly anharmonic potentials, leading to increased Umklapp scattering. If the guests only partially occupy the open sites, point defect scattering will also arise.[32] The effect of guest atoms on $v_s$ will be dictated by the relative change in density and elastic modulus; we would expect that light guest species may actually increase $v_s$ by stiffening the lattice without dramatically altering the density. In contrast, heavy, weakly bound atoms should lower $v_s$.

Much of the excitement surrounding skutterudites and clathrates has been focused on the prediction[66] and observation[67–69] of a phenomena termed "rattling", observed when the guest atom is under-constrained and weakly bound. Experimentally, materials in which guest atoms are strong rattlers are found to exhibit extremely low $\kappa_L$.[68,70] While it is widely accepted that rattling atoms result in strongly localized modes within the acoustic frequency range, the mechanism by which rattler modes reduce $\kappa_L$ is under debate. Historically, the reduction in $\kappa_L$ has been attributed to resonant scattering by the guest atom.[71] However, the impact of rattling on the group velocity has recently been recognized as an alternative explanation of the low experimental $\kappa_L$.[72,73]

Resonant scattering treats the guest atom vibrations as uncorrelated with respect to the framework and other guest species. This scattering mechanism was originally proposed to explain a low temperature indentation in $\kappa_L$ observed in a solid solution of KCl and $KNO_2$.[74,75] Fig. 8(a) shows the combined effects of resonant and Umklapp scattering for two different resonant scattering constants. Here, $\sigma$ is reduced in a narrow frequency range about $\omega_o$, the frequency of the guest atom vibrational mode. This resonant scattering model has successfully been

used to explain the unusual temperature dependence of $\kappa_L$ for both clathrates and skutterudites.[71,76] However, these models assume a constant group velocity, which fails to capture the complexity of the phonon dispersion and the interaction of the rattling and acoustic modes.

The phonon dispersions of these framework compounds can be investigated using a modified BvK model. We can approximate an empty framework as a monatomic chain of atoms with mass $m_1$ connected with springs $k_1$ (black curve, Fig. 8(b)). To simulate the inclusion of guest atoms, we include a second atom with mass $m_2$ which is coupled to the framework via springs ($k_2$), as shown in Fig. 8(b). At the limit of $k_2 \gg k_1$, the lattice behaves as a 2-atom solid with acoustic and optical modes similar to those discussed above in the mass-contrast section.

However, when $k_2 \ll k_1$, the guest species is only loosely bound in the framework and the associated optical mode drops into the same frequency range as the acoustic branch. The interaction of these two modes is manifested as the "avoided crossing" shown in Fig. 8(b) for a range of $k_2 : k_1$ ratios. For this model, we have fixed the framework properties ($k_1$ and $m_1$) and the frequency of the rattler mode ($\omega_o \sim \sqrt{k_2/m_2}$). As $k_2$ stiffens, increased mode mixing is observed. This mixing results in a local reduction of $v_g(\omega)^2$, as illustrated by Fig. 8(c).

The local reduction in group velocity near $\omega_o$ has been experimentally observed through inelastic neutron scattering experiments. Measurements of the phonon dispersion of $Ba_8Ga_{16}Ge_{30}$ and $CeRu_4Sb_{12}$ single crystals confirm the presence of rattler modes within the acoustic branch and coupling between these modes.[73,77] In contrast, phonon dispersion measurements of $CeOs_4Sb_{12}$ reveal a conspicuous lack of rattling modes in the acoustic branch. The extremely high framework density, and corresponding low $v_s$, of $CeOs_4Sb_{12}$ appears to result in acoustic branches that do not reach the guest mode frequency.[78]

Measurements of the heat capacity, phonon density of states and Raman spectra may also be used to observe low frequency guest modes.[67,79–83] The flatness of the guest mode can be deduced from the width of the heat capacity or phonon DOS peak. For example, in the germanium-clathrates, broad peaks observed in the phonon DOS reveal strong coupling between the guest and host modes.[84] Note that while these techniques reveal features in the phonon dispersion, they are insensitive to phonon scattering effects.

Complimenting this experimental work is an increasing body of computational studies which attempt to understand rattling behavior.[81,85–87] The ability to predict the frequency of the rattler mode for different guest species is a particularly attractive feature of this work, helping to guide development of skutterudites with multiple guest elements.[88]

Despite the vast body of research concerning rattling modes, there is an ongoing debate in the community: Is resonant scattering or a local reduction in $v_g$ near the avoided crossing the dominant cause of low $\kappa_L$? Fig. 8(d) illustrates the difficulty of distinguishing between these two effects. As a baseline, $\kappa_s(\omega)$ of an empty framework is calculated using $\sigma_U$ and $\sigma_B$ and a single-atom, 1-D BvK model for $v_g(\omega)$ (curve A). If resonant scattering is included, a dramatic reduction of $\kappa_s(\omega)$ occurs near $\omega_o$ (curve B). However, a similar reduction of $\kappa_s(\omega)$ can be achieved by simply accounting for the reduction in group velocity near $\omega_o$ (curve C).[72] Temperature dependent measurements may not be able to distinguish between these effects, as both models in Fig. 8(d) can be used to reproduce the characteristic indentation in $\kappa_L$ seen in some filled framework materials. It is clear that frequency-dependent measurements of $v_g(\omega)$ and $\sigma(\omega)$ will be vital to unravel these intertwined effects on $\kappa_L$.

## Conclusion

Rational design strategies now exist to guide the discovery and development of advanced thermal materials, heralding a new era for energy materials. Disorder on multiple length scales, from point defects to crystal boundaries, can be used to scatter phonons of different frequencies. Equally influential is the structural complexity of the unit cell, which traps heat in low velocity phonon modes. Resonant phonon modes from "rattling" atoms can be used to reduce the velocity of the remaining acoustic phonons. Despite the intricacies of phonon transport in such complex materials, we find that the thermal behavior can be explained by relatively simple models. These models stress the fundamental *material parameters* which ultimately determine thermal conductivity.

## References

1 P. G. Klemens and M. Gell, Thermal conductivity of thermal barrier coatings, *Mater. Sci. Eng.*, 1998, **A245**, 143–149.

2 C. Levi, Emerging materials and processes for thermal barrier systems, *Curr. Opin. Solid State Mater. Sci.*, 2004, **8**, 77–91.

3 D. R. Clarke, Materials selection guidelines for low thermal conductivity in thermal barrier coatings, *Surf. Coat. Technol.*, 2003, **163–164**, 67–74.

4 C. Wood, Materials for thermoelectric energy conversion, *Rep. Prog. Phys.*, 1988, **51**, 459–539.

5 J. R. Sootsman, D. Y. Chung and M. G. Kanatzidis, New and old concepts in thermoelectric materials, *Angew. Chem., Int. Ed.*, 2009, **48**, 8618–8639.

6 G. Chen, M. S. Dresselhaus, G. Dresselhaus, J.-P. Fleurial and T. Caillat, Recent developments in thermoelectric materials, *Int. Mater. Rev.*, 2003, **48**, 45–66.

7 G. J. Snyder and E. S. Toberer, Complex thermoelectric materials, *Nat. Mater.*, 2008, **7**, 105.

8 E. S. Toberer, A. F. May and G. J. Snyder, Zintl chemistry for designing high efficiency thermoelectric materials, *Chem. Mater.*, 2010, **22**, 624–634.

9 C. B. Vining, W. Laskow, J. O. Hanson, R. R. V. der Beck and P. D. Gorsuch, Thermoelectric properties of pressure-sintered $Si_{0.8}Ge_{0.2}$ thermoelectric alloys, *J. Appl. Phys.*, 1991, **69**.

10 P. Yanzhong, A. Lalonde, S. Iwanaga and G. J. Snyder, High thermoelectric figure of merit in heavy-hole dominated PbTe., *Energy Environ. Sci.*, 2011.

11 Y. Z. Pei, *et al.* Synthesis and thermoelectric properties of $KyCo_4Sb_{12}$, *Appl. Phys. Lett.*, 2006, **89**, 221107.

12 C. A. Cox, *et al.* Structure, heat capacity, and high-temperature thermal properties of $Yb_{14}Mn_{1−x}Al_xSb_{11}$, *Chem. Mater.*, 2009, **21**, 1354–1360.

13 A. Zevalkink, E. S. Toberer, W. Zeier, E. Flage-Larsen and G. J. Snyder, $Ca_3AlSb_3$: an inexpensive, non-toxic thermoelectric material for waste heat recovery, *Energy Environ. Sci.*, 2011, **4**, 510–518.

14 A. F. May, E. S. Toberer, A. Saramat and G. J. Snyder, Characterization and analysis of thermoelectric transport in n-type $Ba_8Ga_{16−x}Ge_{30−x}$, *Phys. Rev. B: Condens. Matter Mater. Phys.*, 2009, **80**, 125205.

15 E. S. Toberer, *et al.* Traversing the metal-insulator transition in a Zintl phase: rational enhancement of thermoelectric efficiency in $Yb_{14}Al_xMn_{1−x}Sb_{11}$, *Adv. Funct. Mater.*, 2008, **18**, 2795.

16 G. S. Nolas, J. L. Cohn, G. A. Slack and S. B. Schujman, Semiconducting Ge clathrates: Promising candidates for

thermoelectric applications, *Appl. Phys. Lett.*, 1998, **73**, 178.

17 C. Uher. & T. M. Tritt, *Skutterudites: Prospective novel thermoelectrics*, 2001, vol. 69, Academic Press, San Diego.

18 M. R. Winter and D. R. Clarke, Oxide materials with low thermal conductivity, *J. Am. Ceram. Soc.*, 2007, **90**, 533540.

19 A. Ward, D. A. Broido, D. A. Stewart and G. Deinzer, Ab initio theory of the lattice thermal conductivity in diamond, *Phys. Rev. B: Condens. Matter Mater. Phys.*, 2009, **80**, 125203.

20 A. Ward and D. A. Broido, Intrinsic phonon relaxation times from first principle studies of the thermal conductivity of Si and Ge, *Phys. Rev. B: Condens. Matter Mater. Phys.*, 2010, **81**, 085205.

21 J. An, A. Subedi and D. J. Singh, Ab initio phonon dispersions for PbTe, *Solid State Commun.*, 2008, **148**, 417–419.

22 J. Dong, O. F. Sankey and C. W. Myles, Theoretical study of the lattice thermal conductivity in Ge framework semiconductors, *Phys. Rev. Lett.*, 2001, **86**, 2361.

23 N. de Koker, Thermal conductivity of MgO periclase from equilibrium first principles molecular dynamics, *Phys. Rev. Lett.*, 2009, **103**, 125902.

24 N. Bernstein, J. L. Feldman and D. J. Singh, Calculations of dynamical properties of skutterudites: Thermal conductivity, thermal expansivity, and atomic mean-square displacement, *Phys. Rev. B: Condens. Matter Mater. Phys.*, 2010, **81**, 134301.

25 R. Berman, *Thermal conduction in solids*, Oxford University Press, Oxford, 1976.

26 *Thermal conductivity: Theory, properties, and applications*, ed. T. M. Tritt, Springer, New York, 2005.

27 D. G. Cahill and R. O. Pohl, Lattice vibrations and heat transport in crystals and glasses, *Annu. Rev. Phys. Chem.*, 1988, **39**, 93–121.

28 G. A. Slack, *Solid State Physics*, 1979, vol. 34, Academic Press, New York.

29 C. J. Vineis, A. Shakouri, A. Majumdar and M. G. Kanatzidis, Nanostructured Thermoelectrics: Big Efficiency Gains from Small Features, *Adv. Mater.*, 2010, **22**, 3970–3980.

30 S. K. Bux, J.-P. Fleurial and R. B. Kaner, Nanostructured materials for thermoelectric applications, *Chem. Commun.*, 2010, **46**, 8311–8324.

31 A. J. Minnich, M. S. Dresselhaus, Z. F. Ren and G. Chen, Bulk nanostructured thermoelectric materials: current research and future prospects, *Energy Environ. Sci.*, 2009, **2**, 466–479.

32 G. P. Meisner, D. T. Morelli, S. Hu, J. Yang and C. Uher, Structure and lattice thermal conductivity of fractionally filled skutterudites: Solid solutions of fully filled and unfilled end members, *Phys. Rev. Lett.*, 1998, **80**, 3551–3554.

33 J. Callaway, Model for lattice thermal conductivity at low temperatures, *Phys. Rev.*, 1959, **113**, 1044–1051.

34 M. G. Holland, Analysis of lattice thermal conductivity, *Phys. Rev.*, 1963, **132**, 2461–2471.

35 P. G. Klemens, Theory of Thermal Conductivity in Solids, in *Thermal Conductivity*, ed. R. P. Tye, 1969, Vol. 1, Academic Press, London.

36 C. Dames and G. Chen, Thermal conductivity of nanostructured thermoelectric materials, in *CRC Handbook of Thermoelectrics*, 2006, CRC Press.

37 D. M. Rowe, V. S. Shukla and N. Savvides, Phonon scattering at grain boundaries in heavily doped fine-grained silicon-germanium alloys, *Nature*, 1981, **290**, 765–766.

38 C. Kittel, *Introduction to Solid State Physics*, 1986, John Wiley and Sons Inc., New York.

39 J. D. Chung, A. J. H. McGaughey and M. Kaviany, Role of phonon dispersion in lattice thermal conductivity modeling, *J. Heat Trans.*, 2004, **126**, 691–696.

40 P. G. Klemens, Thermal conductivity and lattice vibrational modes, *Solid State Phys - Adv. Res. Appl.*, 1972, **7**, 1–98.

41 M. A. Black, Thermal conductivity and anharmonic forces, *Am. J. Phys.*, 1972, **41**, 691–696.

42 J. S. Dugdale and D. K. C. MacDonald, Lattice thermal conductivity, *Phys. Rev.*, 1955, **98**, 1751–1752.

43 M. Roufosse and P. G. Klemens, Thermal-conductivity of complex dielectric crystals, *Phys. Rev. B: Solid State*, 1973, **7**, 5379–5386.

44 G. Leibfried and E. Schloemann, Thermal conductivity of dielectric solids by a variational technique, *Nachr. Akad. Wiss. Goettingen, Math.-Phys. Kl., 2A: Math.-Phys.-Chem. Abt.*, 1954, **23**, 1366–1370.

45 C. L. Julian, Theory of heat conduction in rare-gas crystals, *Phys. Rev.*, 1965, **137**, A128–A137.

46 G. A. Slack and S. Galginaitis, Thermal conductivity and phonon scattering by impurities in CdTe, *Phys. Rev.*, 1964, **133**, A253–A268.

47 H. Wang, Y. Pei, A. D. LaLonde and G. J. Snyder, Heavily doped p-type PbSe with high thermoelectric performance: an alternative of PbTe, *Adv. Mater.*, 2011, **23**, 1366.

48 H. J. Goldsmid and A. W. Penn, Boundary scattering of phonons in solid solutions, *Phys. Lett.*, 1968, **27A**, 523–524.

49 J. E. Parrott, The thermal conductivity of sintered semiconductor alloys, *J. Phys. C: Solid State Phys.*, 1969, **2**, 147–151.

50 S. K. Bux, *et al.* Nanostructured bulk silicon as an effective thermoelectric material, *Adv. Funct. Mater.*, 2009, **19**, 2445–2452.

51 P. G. Klemens, The scattering of low-frequency lattice waves by static imperfections, *Proc. Phys. Soc., London, Sect. A*, 1955, **68**, 1113.

52 M. Blackman, On the heat conduction of simple cubic crystals, *Philos. Mag.*, 1935, **19**, 989.

53 M. Born and T. V. Kármán, *Physik Z.*, 1912, **13**, 297.

54 S. Pettersson, Calculation of the thermal conductivity of alkali halide crystals, *J. Phys. C: Solid State Phys.*, 1987, **20**, 1047–1061.

55 E. F. Steigmeier and I. Kudman, Acoustical-optical phonon scattering in Ge, Si, and iii-v compounds, *Phys. Rev.*, 1966, **141**, 767.

56 C. J. Friedrich, R. Gadow and M. H. Lischka, Lanthanum hexaaluminate thermal barrier coatings, *The 25th An. Int. Conf. on Composites, Advanced Ceramics, Materials, and Structures: B*, 2001, 375–382.

57 T. Takeuchi, N. Nagasako, R. Asahi and U. Mizutani, Extremely small thermal conductivity of the Al-based Mackay-type 1/1-cubic approximants, *Phys. Rev. B: Condens. Matter Mater. Phys.*, 2006, **74**, 054206.

58 E. S. Toberer, A. Zevalkink, N. Crisosto and G. J. Snyder, The Zintl compound $Ca_5Al_2Sb_6$ for low-cost thermoelectric power generation, *Adv. Funct. Mater.*, 2010, **20**, 4375–4380.

59 S. R. Brown, S. M. Kauzlarich, F. Gascoin and G. J. Snyder, High-temperature thermoelectric studies of $A_{11}Sb_{10}$ (A = Yb, Ca), *J. Solid State Chem.*, 2007, **180**, 1414.

60 T. Yi, C. A. Cox, G. J. Snyder and Kauzlarich, High-temperature transport of the Zintl phases $Yb_{11}GaSb_9$ and $Yb_{11}InSb_9$, *Chem. Mater.*, 2010, **22**, 935–941.

61 N. P. Padture and P. G. Klemens, Low thermal conductivity in garnets, *J. Am. Ceram. Soc.*, 1997, **80**, 1018–1020.

62 R. Bruls, H. T. Hintzen and R. Metselaar, On the Debye temperature in the Slack approximation for an estimation of the thermal conductivity of nonmetallic compound, *J. Appl. Phys.*, 2005, **98**, 126101.

63 G. A. Slack. *The thermal conductivity of nonmetallic crystals*, 1979, vol. 34, Academic Press, New York.

64 D. G. Cahill, S. K. Watson and R. O. Pohl, Lower limit to the thermal conductivity of disordered crystals, *Phys. Rev. B: Condens. Matter*, 1992, **46**, 6131–6140.

65 Note that, for most phonon frequencies, $I_{glass} = \lambda/2$ is still much larger than the average distance between atoms. See G. D. Mahan, *Solid State Physics,* 1998, Academic Press, New York.

66 G. A. Slack and V. G. Tsoukala, Some properties of semiconducting $IrSb_3$, *J. Appl. Phys.*, 1994, **76**, 1665–1671.

67 V. Keppens, *et al.* Localized vibrational modes in metallic solids, *Nature*, 1998, **395**, 876–878.

68 B. C. Sales, B. C. Chakoumakos, D. Mandrus and J. W. Sharp, Atomic displacement parameters and the lattice thermal conductivity of clathrate-like thermoelectric compounds, *J. Solid State Chem.*, 1999, **146**, 528–532.

69 M. Christensen, N. Lock, J. Overgaard and B. B. Iversen, Crystal structures of thermoelectric n- and p-type $Ba_8Ga_{16}Ge_{30}$ studied by single crystal, multi-temperature, neutron diffraction, conventional X-ray diffraction and

resonsant X-ray diffraction, *J. Am. Chem. Soc.*, 2006, **128**, 15657–15665.

70 P. F. Qiu, *et al.* High-Temperature electrical and thermal transport properties of fully filled skutterudites RFe$_4$Sb$_{12}$ (R = Ca, Sr, Ba, La, Ce, Pr, Nd, Eu, and Yb), *J. Appl. Phys.*, 2011, **109**, 063713.

71 J. L. Cohn, G. S. Nolas, V. Fessatidis, T. H. Metcalf and G. A. Slack, Glasslike heat conduction in high-mobility crystalline semiconductors, *Phys. Rev. Lett.*, 1999, **82**, 779.

72 M. Zebarjadi, K. Esfarjani, J. Yang, Z. F. Ren and G. Chen, Effect of filler mass and binding on thermal conductivity of fully filled skutterudites, *Phys. Rev. B: Condens. Matter Mater. Phys.*, 2010, **83**, 195207.

73 M. Christensen, *et al.* Avoided crossing of rattler modes in thermoelectric materials, *Nat. Mater.*, 2008, **7**, 811–815.

74 R. O. Pohl, Thermal conductivity and phonon resonant scattering, *Phys. Rev. Lett.*, 1962, **8**, 481–483.

75 M. Wagner, Influence of localized modes on thermal conductivity, *Phys. Rev.*, 1963, **131**, 1443–1455.

76 J. Yang, *et al.* Effect of Sn substituting for Sb on the low temperature transport properties of Ytterbium-filled skutterudites, *Phys. Rev. B: Condens. Matter*, 2003, **67**, 165207.

77 C. H. Lee, I. Hase, H. Sugawara, H. Yoshizawa and H. Sato, Low-lying optical phonon modes in the filled skutterudite CeRu$_4$Sb$_{12}$, *J. Phys. Soc. Jpn.*, 2006, **75**, 123602.

78 C. P. Yang, *et al.* Phonon dispersion curves in CeOs$_4$Sb$_{12}$, *J. Phys.: Condens. Matter.*, 2007, **19**, 225214.

79 M. Beekman, R. P. Hermann, A. M. Mochel, F. Juranyi and G. S. Nolas, A study of low-energy guest phonon modes in clathrate-II Na$_x$Si$_{136}$ (x = 3, 23, and 24), *J. Phys.: Condens. Matter*, 2010, **22**, 355401.

80 M. M. Koza, *et al.* Breakdown of phonon glass paradigm in La- and Ce-filled Fe$_4$Sb$_{12}$ skutterudites, *Nat. Mater.*, 2008, **7**, 805–810.

81 M. M. Koza, *et al.* Vibrational dynamics of the type-I clathrate Ba$_8$Zn$_x$Ge$_{46-x-y}\square_y$ (x = 0,2,4,6,8), *Phys. Rev. B: Condens. Matter Mater. Phys.*, 2010, **82**, 214301.

82 Y. Takasu, *et al.* Off-center rattling and cage vibration of the carrier-tuned type-I clathrate Ba$_8$Ga$_{16}$Ge$_{30}$ studied by Raman scattering, *Phys. Rev. B: Condens. Matter Mater. Phys.*, 2010, **82**, 134302.

83 G. S. Nolas, *et al.* Raman scattering study of stoichiometric Si and Ge type II clathrates, *J. Appl. Phys.*, 2002, **92**, 7225–7230.

84 R. P. Hermann, *et al.* Neutron and nuclear inelastic scattering study of the Einstein oscillators in Ba-, Sr-, and Eu-filled germanium clathrates, *Phys. Rev. B: Condens. Matter Mater. Phys.*, 2005, **72**, 174301.

85 C. W. Myles, K. Biswas and E. N. Nenghabi, Guest "rattling" impurities in Si and Ge clathrate semiconductors, *Phys. B*, 2007, **401402**, 695–698.

86 E. N. Nenghabi and C. W. Myles, First-principles calculations of the vibrational and thermal properties of the type-I clathrates Ba$_8$Ga$_{16}$Si$_x$Ge$_{30-x}$ and Sr$_8$Ga$_{16}$Si$_x$Ge$_{30-x}$, *Phys. Rev. B: Condens. Matter Mater. Phys.*, 2008, **78**, 195202.

87 N. P. Blake, S. Latturner, J. D. Bryan, G. D. Stucky and H. Metiu, Band structures and thermoelectric properties of the clathrates Ba$_8$Ga$_{16}$Ge$_{30}$, Sr$_8$Ga$_{16}$Ge$_{30}$, Ba$_8$Ga$_{16}$Si$_{30}$, and Ba$_8$In$_{16}$Sn$_{30}$, *J. Chem. Phys.*, 2001, **115**, 8060–8073.

88 J. Yang, W. Zhang, S. Q. Bai, Z. Mei and L. D. Chen, Dual-frequency resonant phonon scattering in Ba$_x$R$_y$Co$_4$Sb$_{12}$ (R = La, Ce, and Sr), *Appl. Phys. Lett.*, 2007, **90**, 192111.